Individual Polymer Paths and End-Point Stretching in Polymer Brushes

Christian Seidel* and Roland R. Netz

Max-Planck-Institut für Kolloid- und Grenzflächenforschung,† Am Mühlenberg, D-14476 Golm, Germany

Received October 9, 1999; Revised Manuscript Received November 1, 1999

ABSTRACT: Molecular dynamics simulations and self-consistent field calculations have been used to study average polymer paths of end-grafted, strongly overlapping polymers in a good solvent. Contrary to what is usually assumed, and in agreement with earlier classical and self-consistent field results, we find the end points of average polymer paths which end at a certain distance from the grafting surface to be stretched. The agreement between simulations and self-consistent calculations clearly demonstrates that end-point stretching effects, appearing for the experimentally relevant case of finite-length and finitely stretched polymers, are not suppressed by fluctuations.

I. Introduction

Polymer chains in a good solvent that are terminally attached to a grafting surface form a strongly stretched polymer brush at high enough surface coverage. Technical applications of such brushes range from colloidal stabilization and lubrication, to surface modification. Theoretical interest in these systems was spurned when Zhulina et al.[1] and Milner et al.[2] found that these brushes show a parabolic density profile. These calculations are valid in the infinite-stretching limit (ISL), which corresponds to the limit of infinitely long polymers. In the ISL calculations, the stretching of the free polymer ends was assumed to be zero. This is commonly interpreted as a consequence of the free polymer end not being subjected to an external force. However, subsequent calculations performed in the classical approximation, which relaxed the constraint of infinitely long polymer chains, found the free ends to be stretched.[3] This result was later confirmed by self-consistent field (SCF) calculations,[4] and it was shown that the end-point tension of individual polymer paths vanishes in the asymptotic limit of infinite stretching. The initial assumption of vanishing end-point tension in the ISL calculations is therefore justified (but only in that asymptotic limit). Nevertheless, the question of the end-point stretching of anchored polymers of finite length is clearly of conceptual importance and possibly of experimental relevance.

During the past decade a large number of experimental studies have been carried out to check the theoretical predictions. In particular, the interest was focused on the scaling of the brush height h and the internal structure of the brushes. Small-angle neutron scattering[5] and neutron reflectivity[6] data were satisfactorily fitted to parabolic density profiles complemented by, e.g., an exponential tail. In addition to neutron scattering and reflectivity experiments, surface force measurements[7] have shown good agreement with the predicted scaling behavior[8] $h \sim N\rho_a^{1/3}$, with N being the chain length or polymerization index and ρ_a the anchoring density.

The scaling law and parabolic density profile were also qualitatively confirmed by (i) direct numerical solutions of the self-consistent[9,10] or classical[11] equations, performed for polymer chains of finite length, and (ii) computer simulations using both molecular dynamics (MD) and Monte Carlo methods (MC) (see, e.g., ref 12 and references therein). Previous computer simulations, however, did not pay any special attention to the end-point stretching. The mean path, obtained by averaging over all polymer paths regardless of their end-point position, was discussed in a few studies. However, as seen from SCF calculations[4] the end-point stretching can be actually rather small for the mean path with end points averaged over, even though it is not small for the average paths with some fixed end point. Indeed, simulation results on the average polymer paths obtained by Laradji, Guo, and Zuckermann[13] within a model restricted to quadratic interaction agree quite well with the ISL predictions, particularly for high values of N and ρ_a. On the other hand, in models with higher order interactions the agreement is less convincing[14] or even poor, particularly for high values of ρ_a[15] (presumably also due to the relatively short chains used in the latter simulation study).

In this paper, we compare SCF predictions with MD results to test whether end-point stretching is obtained in the presence of fluctuations. We indeed find the MD behavior in close agreement with the predictions by SCF methods. This agreement clearly demonstrates that end-point stretching effects, appearing for the experimentally relevant case of finite-length and finitely stretched polymers, are not suppressed by fluctuations.The organization of the paper is as follows: In section II we present a short summary of the SCF methods and results. We also present some general arguments showing that polymer end points are in general stretched if the averaging is only done over a certain subset of all possible paths. Section III is devoted to a short description of the simulation model and method. In section IV we discuss simulation results and compare them with SCF predictions. Finally, we conclude with a suggestion for an experiment to measure the end-point stretching in brush systems.

II. Self-Consistent Field Theory

We briefly review the model and the methods used for the SCF calculation (for a more detailed discussion, see ref 4). The partition function for M end-grafted

* To whom correspondence should be addressed.
† Mailing address: D-14424 Potsdam, Germany.

10.1021/ma981582w CCC: $19.00
Published on Web 01/05/2000

Gaussian polymers which interact via a quadratic repulsion of strength w is

$$Z = \prod_{\alpha=1}^{M}\left[\int D\mathbf{r}_\alpha(\cdot)\exp\left\{-\frac{3}{2a^2}\int_0^N \dot{\mathbf{r}}_\alpha{}^2(s)\,\mathrm{d}s\right\}\right]\times \exp\left\{-\frac{w}{2}\int \rho^2(\mathbf{r})\,\mathrm{d}\mathbf{r}\right\} \quad (1)$$

where a denotes the Kuhn length, and the local monomer density $\rho(\mathbf{r})$ is defined by

$$\rho(\mathbf{r}) = \sum_{\alpha=1}^{M}\int_0^N \mathrm{d}s\;\delta[\mathbf{r} - \mathbf{r}_\alpha(s)] \quad (2)$$

It is implicitly assumed that all polymer paths $\mathbf{r}_\alpha(s)$ start from a planar grafting surface which is impenetrable, so that they are confined to a half space. The Gaussian expression for the polymer elasticity is, of course, only valid for polymers which are not stretched to their contour length, which, however, does not severely restrict the applicability of the model.[4] More serious is the restriction in eq 1 to the second virial coefficient. Higher order terms in the density become important when the system is near the θ point, and wherever the monomer density is expected to be large, such as in the vicinity of the grafting surface. We will discuss this point in more detail when we compare the SCF results with the MD results.

The SCF theory can be formally obtained by a saddle-point approximation, and it amounts to neglecting correlation effects due to density fluctuations. In the mean-field limit, there is a single typical length scale h_0 given by

$$h_0 \equiv N(2w\rho_a a^2/3)^{1/3} \quad (3)$$

where the anchoring density is defined by $\rho_a = M/A$ (the number of grafted chains per area A). The length scale h_0 corresponds to the scaling prediction for the brush height.[8] To make the discussion more transparent, we introduce dimensionless coordinates $\tilde{\mathbf{r}} = \mathbf{r}/h_0$. After proper rescaling and normalization, the theory depends on a single parameter β, defined as

$$\beta \equiv N\left(\frac{3w^2\rho_\alpha{}^2}{2a^2}\right)^{1/3} = \frac{3}{2}\left(\frac{h_0}{R_0}\right)^2 \quad (4)$$

which is proportional to the square of the ratio of the length scale h_0 to the Flory radius of a free Gaussian polymer $R_0 = aN^{1/2}$. Note that the simulations discussed below model polymers in a good solvent. In order to compare the SCF results with those of the simulations, we take the intrachain interactions into account in a more heuristic way by using the free polymer radius R_F, measured from simulations of single reference chains, instead of the Gaussian R_0. The mean-field free energy per polymer chain is

$$F_{mf} = -\frac{\beta}{2}\int \phi(\tilde{z})^2\,\mathrm{d}\tilde{z} - \ln Q[\phi] \quad (5)$$

where $\phi(\tilde{z})$ is the normalized density distribution. The single polymer partition function is

$$Q[\phi] = \int_0^\infty D\tilde{z}(\cdot)\exp\{-\beta\int_0^1(\dot{\tilde{z}}^2(t) + \phi[\tilde{z}(t)])\,\mathrm{d}t\} \quad (6)$$

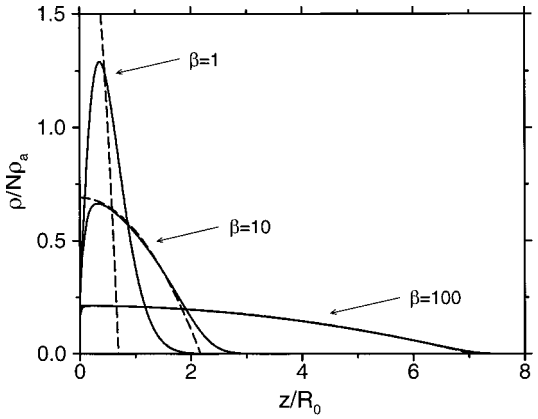

Figure 1. Theoretical results for the rescaled monomer number density, $(3/2\beta)^{1/2}\phi = \rho/N\rho_a$, as a function of the rescaled distance from the grafting surface z/R_0 for $\beta = 1, 10, 100$. Shown are both the results of the (finite stretching) SCF theory (solid lines) and those in the infinite-stretching limit (dashed lines).

and the polymer density profile is determined by the self-consistent equation

$$\phi(\tilde{z}) = -\frac{\delta \ln Q[\phi]}{\delta\beta\,\phi(\tilde{z})} \quad (7)$$

Numerically, the single polymer partition function is evaluated by a discretized path integral, and the self-consistent equation is then solved with some suitable relaxation algorithm. We point out that we evaluate the partition function in the continuum limit.[4] In Figure 1 we show results for the density profile for three different values of the stretching parameter β. For increasing β, the SCF density profiles approach the ISL result (plotted in thick dashed lines). In fact, for $\beta = 100$, the SCF result is indistinguishable from the ISL prediction. For moderate stretching, $\beta = 10$, the SCF and ISL results show pronounced differences; specifically, the SCF profiles exhibit an exponentially decaying tail.

In order to compare the SCF results with that of the simulation, let us define an effective stretching parameter γ as the relation between the SCF average end-point height $\langle z_e\rangle = \langle z(t{=}1)\rangle$ and that for a noninteracting Gaussian polymer anchored at an impenetrable wall $\langle z_e\rangle_0$

$$\gamma = \frac{\langle z_e\rangle}{\langle z_e\rangle_0} \quad (8)$$

Note that the effective stretching parameter is also of experimental interest. The normalized segment probability amplitude for a noninteracting anchored polymer can be calculated by the method of images and is given by[4]

$$q_t(z) = \frac{3}{t}\frac{z}{R_0{}^2}\exp\left\{-\frac{3}{2t}\frac{z^2}{R_0{}^2}\right\} \quad (9)$$

The average end-point distance for the anchored Gaussian noninteracting polymer is obtained by a weighted average to give

$$\langle z_e\rangle_0 = \int_0^\infty \mathrm{d}z\; zq_1(z) = R_0\sqrt{\frac{\pi}{6}} \quad (10)$$

The dependence of the effective stretching parameter

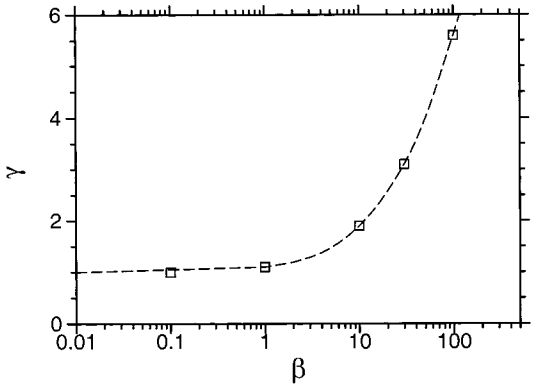

Figure 2. Effective stretching ratio γ as defined in eq 8 versus stretching parameter β. SCF results with the dashed line being a guide to the eyes.

γ, eq 8, on the parameter β, following from the SCF theory is shown in Figure 2. As can be seen, for vanishing β the effective stretching parameter γ approaches unity. The curve in Figure 2 will be later used as a gauge in order to estimate the value of β that corresponds to our MD simulations. Also, this curve allows direct comparison with experimental results, since it is typically the parameter γ that can be easily determined in experiments. Of course, the impenetrable wall by itself has an influence on the statistics of a Gaussian polymer and in fact stretches it away from the wall. The mean square end-to-end distance along a certain direction of a free Gaussian polymer is $\langle z^2(t=1)\rangle_{0,\text{free}} = R_0^2/3$. The mean square separation from the impenetrable wall is for a Gaussian polymer given by $\langle z_e^2\rangle_0 = 2R_0^2/3$. For a Gaussian chain, the effect of the wall is therefore to increase the mean square radius in the direction perpendicular to the wall by a factor of 2.

In Figure 3 we plot scaled average polymer paths which end at a certain distance z_e from the wall as well as the mean polymer paths obtained by averaging over all paths. The values of the stretching parameter β are those for which the density profiles are shown in Figure 1. To get an idea of their relative weight, we plot the polymer paths together with the normalized density of free ends $\rho_e(z)$ such that $\int_0^\infty dz\, \rho_e(z) = 1$. We observe the salient feature that paths which end further from the grafting surface than the average path are stretched through their entire length, including their end points, while those paths which end closer to the surface than the average path bend around such that their free ends point toward the surface. This feature is more prominent for smaller values of β. It is worth pointing out that the average path is indeed almost unstretched at its end.

This result is somewhat puzzling, since one would normally expect free polymer ends to be unstretched. To understand the origin of the end-point stretching in a simple manner, let us consider the behavior of noninteracting, Gaussian polymers. The normalized end-point distribution for a Gaussian polymer of length tN which starts at a position $\mathbf{r}_0$ is

$$q_t(\mathbf{r},\mathbf{r}_0) = \left(\frac{3}{2\pi t R_0^{\,2}}\right)^{3/2} \exp\left[-\frac{3}{2}(\mathbf{r}-\mathbf{r}_0)^2/tR_0^{\,2}\right] \quad (11)$$

In fact, $q_t(\mathbf{r},\mathbf{r}_0)$ is the Green function. The end-point distribution is normalized to unity, and the mean square

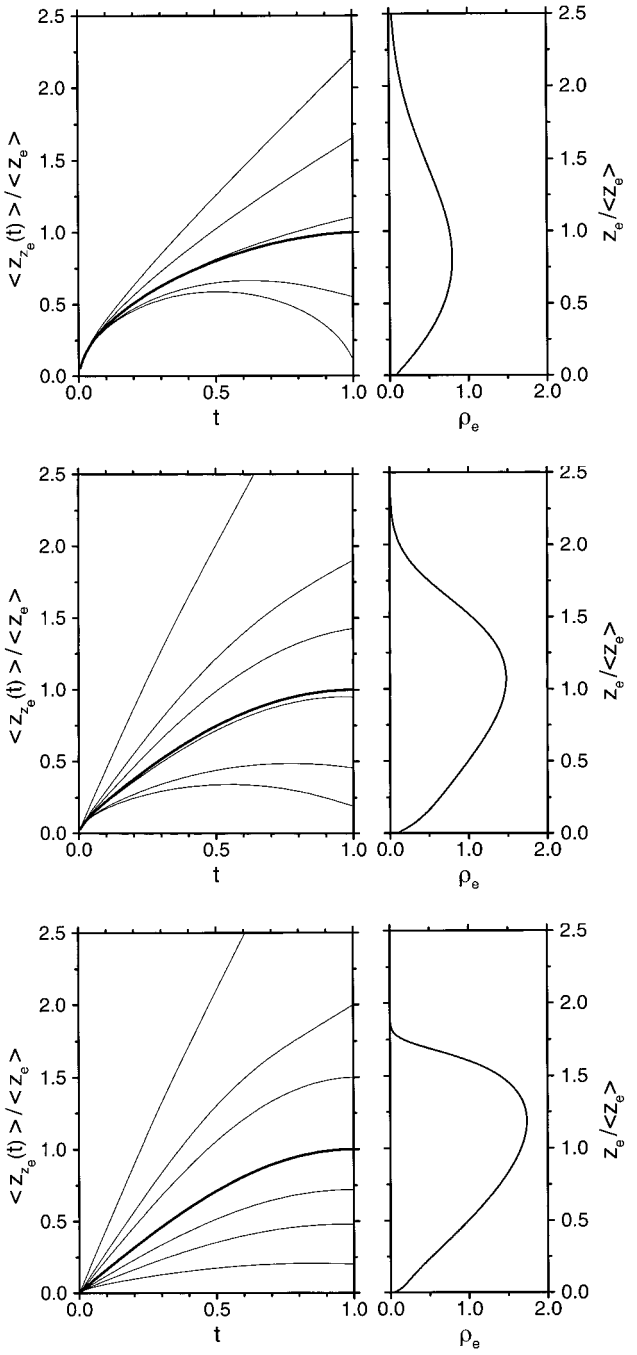

Figure 3. SCF results for average polymer paths which end at a certain distance z_e from the wall (on the left) and for the end-point distribution (on the right) for $\beta = 1$, 10, 100 (from top to bottom), i.e., for $\gamma = 1.1$, 1.9, 5.6 (compare Figure 2). The thick solid lines show the mean paths obtained by averaging over all end-point positions.

end-to-end distance is correctly given by $\langle(\mathbf{r}_t - \mathbf{r}_0)^2\rangle = tR_0^2$. The average path for a polymer of length N with the two end points held fixed at positions $\mathbf{r}_0$ and $\mathbf{r}_1$ can be formulated in terms of the Green function as

$$\langle \mathbf{r}(t)\rangle = \int d\mathbf{r}\; q_t(\mathbf{r},\mathbf{r}_0)\; \mathbf{r}\; q_{1-t}(\mathbf{r},\mathbf{r}_1) \quad (12)$$

The integral can be performed straightforwardly, giving

$$\langle \mathbf{r}(t)\rangle = \mathbf{r}_0 + t(\mathbf{r}_1 - \mathbf{r}_0) \quad (13)$$

As could be expected, the average path is just a straight line, and the polymer is on average uniformly stretched,

including the start and the end point. This simple exercise shows that one should expect polymers to be stretched on average if one only looks at polymers with their end point confined to a certain location, i.e., if one only considers a subset of all possible polymer paths. Going back to the brush problem, it is clear that if one looks only at a subset of polymers which end at a certain distance away from the wall, they should be stretched at their end points. That the end-point stretching changes sign close to the wall is a feature that in fact already results for noninteracting polymers which are anchored at an impenetrable wall.[4] In the following section, we show that this interesting feature is conserved upon addition of fluctuations. This means, in specific, that the nonvanishing end-point stretching should be experimentally observable, as we will discuss in our final section.

III. Simulation Model and Method

We use a polymer molecular dynamics method suggested by Grest and Kremer[16] in which all the chain segments are coupled to a heat bath. This method has been used before to study various polymer problems, including polymer brushes.[17] Each particle i with mass m moves according to a Langevin equation

$$m\frac{\mathrm{d}^2\vec{\mathbf{r}}_i}{\mathrm{d}t^2} = -\vec{\nabla}\cdot U_i - m\Gamma\frac{\mathrm{d}\vec{\mathbf{r}}_i}{\mathrm{d}t} + \vec{\mathbf{W}}_i(t) \qquad (14)$$

where $\vec{\mathbf{r}}_i$ is the position vector of particle i and the friction of the particles with the heat bath is denoted by Γ. U_i is the total potential acting on particle i. The interaction with the solvent is represented by the random force $\vec{\mathbf{W}}_i(t)$, which can be taken as a Gaussian white noise. Due to the fluctuation−dissipation theorem Γ and $\vec{\mathbf{W}}_i$ are coupled and obey the relation

$$\langle \mathbf{W}_i(t)\cdot\mathbf{W}_j(t')\rangle = 6k_\mathrm{B}Tm\Gamma\delta_{ij}\delta(t-t') \qquad (15)$$

where $k_\mathrm{B}T$ is the thermal energy. In our simulation model the total potential U_i has three terms

$$U_i = \sum_{j\neq i}\{U_\mathrm{LJ}(r_{ij}) + U_\mathrm{FENE}(r_{ij})\} + U_\mathrm{w}(z_i) \qquad (16)$$

where r_{ij} is the particle−particle distance $r_{ij} = |\vec{\mathbf{r}}_i - \vec{\mathbf{r}}_j|$ and z_i is the distance of particle i to the grafting surface. The chains are assumed to be in a good solvent, giving rise to a repulsive interaction between the monomers described by a purely repulsive Lennard-Jones potential

$$U_\mathrm{LJ}(r) = \begin{cases} 4\epsilon\left[\left(\frac{\sigma}{r}\right)^{12} - \left(\frac{\sigma}{r}\right)^{6}\right] + \epsilon, & \text{if } r \le r_\mathrm{c} \\ 0, & \text{if } r > r_\mathrm{c} \end{cases} \qquad (17)$$

where r_c is the interaction cutoff, chosen as $r_\mathrm{c} = 2^{1/6}\sigma$. In addition to the Lennard-Jones repulsion, connected monomers interact with a finite extensible nonlinear elastic (FENE) interaction

$$U_\mathrm{FENE}(r) = \begin{cases} -0.5kr_\mathrm{m}^2\ln\left[1 - \left(\frac{r}{r_\mathrm{m}}\right)^2\right], & \text{if } r \le r_\mathrm{m} \\ \infty, & \text{if } r > r_\mathrm{m} \end{cases} \qquad (18)$$

Following previous simulation studies on grafted chains[17] in most of our simulations the parameters are set to $k = 30\epsilon/\sigma^2$, $r_\mathrm{m} = 1.5\sigma$ which gives an average bond length $a \approx 0.97\sigma$. Additionally we make a comparison to data based on simulations with rather extensible chains applying a parameter set used in simulations of polymers in solution,[18] i.e., $k = 7\epsilon/\sigma^2$, $r_\mathrm{m} = 2\sigma$, which gives $a \approx 1.1\sigma$. Although in the latter case bond crossing cannot be neglected in the high-density brush regime, for average quantities considered in the paper we obtain rather good agreement provided the average bond lengths are properly rescaled. To make sure that none of the particles crosses the hard interface at $z = 0$ where the chains are anchored with one of their end segments, a purely repulsive wall potential is taken as

$$U_\mathrm{w}(z) = \begin{cases} \epsilon\left[\left(\frac{\sigma}{z}\right)^n + A_n\frac{z}{\sigma} + B_n\right], & \text{if } z \le 0.5\sigma \\ 0, & \text{if } z > 0.5\sigma \end{cases} \qquad (19)$$

where A_n and B_n are chosen such that both the wall potential and the force vanish at $z = 0.5\sigma$.[17] The exact form of $U_\mathrm{w}(z)$ is arbitrary. One can in principle use any strongly repelling potential. We use potential (19) with $n = 6$, $A_6 = 768$, $B_6 = -448$ and $n = 12$, $A_{12} = 98\,304$, $B_{12} = -53\,248$.

In the simulation box of volume $L \times L \times L_\mathrm{z}$ there are M chains each of which consists of $N + 1$ monomers with $N = 20, 30, 50$. The first monomer of each chain is firmly attached at a random point to the grafting surface. If not stated otherwise, the results we report in the paper were obtained for systems of $M = 50$ chains with the $N + 1$ monomers bound by the strong FENE potential. In the case of $N = 50$ and strong FENE potential the mean square end-to-end distance of identical free chains was found to be $R_\mathrm{F} \equiv \langle(\mathbf{r}_N - \mathbf{r}_0)^2\rangle_\mathrm{free}^{1/2} = 12.55\sigma$. With soft FENE potential and $N = 20$, 30, and 50, we obtain $R_\mathrm{F} = 7.52\sigma$, 9.73σ, and 13.46σ, respectively. The box length L in x- and y-directions was chosen to give anchoring densities $\rho_\mathrm{a} = M/L^2$ from $0.02\sigma^{-2}$ to $0.17\sigma^{-2}$. The box length in the z-direction is set to about $1.5R_\mathrm{max}(N)$, where $R_\mathrm{max}(N)$ is the contour length of a chain of N monomers. The simulations were carried out at a reduced temperature $k_\mathrm{B}T/\epsilon = 1.2$. Furthermore, we use units in which $m = 1$. Setting the length scale by using the characteristic Kuhn length of a flexible polymer, we have $\sigma \approx a \approx 10$ Å. Hence, the anchoring densities studied by simulations fulfill 2×10^{-4} Å^{-2} < $\rho_\mathrm{a} < 1.7 \times 10^{-3}$ Å^{-2}, a range which is quite comparable to that realized in experimental studies. With a typical size of a chemical monomer $a_0 \approx 2.5$ Å, the number of monomers per Kuhn length becomes $n_0 \approx (a/a_0)^{1/\nu_0} \approx 10$, where the roughness of the freely jointed chain is estimated from the large-q limit of the spherically averaged structure factor $S(q)$ to be $\nu_0 \approx 0.6$. Thus, the chemical polymerization index $\tilde{N} = n_0 \times N$ is $200 < \tilde{N} < 500$. Referring to, e.g., polystyrene, this corresponds to a molecular weight $20\,000 < M_\mathrm{w} < 50\,000$, a range which is also in a reasonable agreement with experimental studies.

The equations of motion of the monomers were numerically integrated using a velocity-Verlet algorithm with a time step δt, chosen as large as possible, while keeping the integration stable. We used $\delta t = 0.002\tau - 0.004\tau$ where the Lennard-Jones time is given by $\tau = \sigma(m/\epsilon)^{1/2}$. Note that the time step δt cannot be mapped directly onto a microscopic time scale, because a single monomer in the model corresponds to several real chemical monomers. The friction coefficient Γ was set to $\Gamma = 1.0\tau^{-1}$. The starting configurations consist of chains fully stretched perpendicular to the grafting

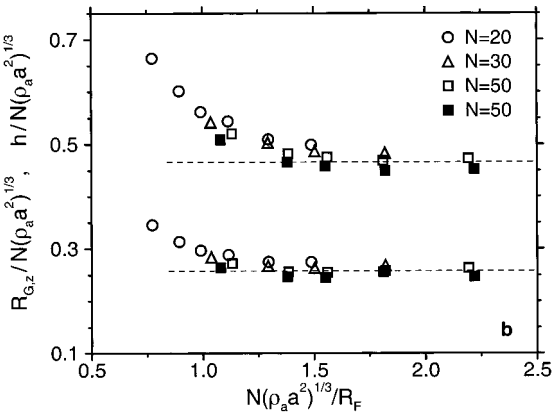

Figure 4. Simulation results for the rescaled average monomer height $h/N(\rho_a a^2)^{1/3}$ (a) and z-contribution to the radius of gyration $R_{G,z}/N(\rho_a a^2)^{1/3}$ (b) versus $N(\rho_a a^2)^{1/3}/R_F$ (full symbols $M = 50$, strong FENE; open symbols $M = 6$, weak FENE).

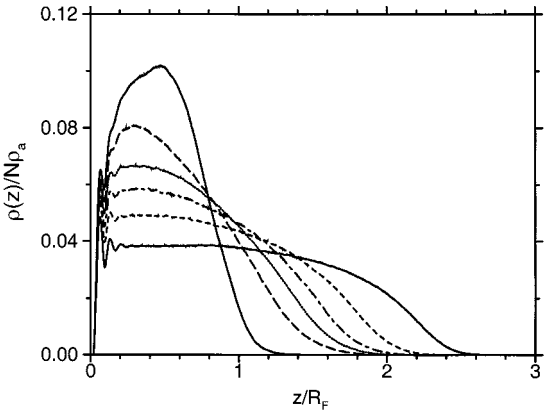

Figure 5. Monomer number density per chain, $\rho(z)/N\rho_a$, as a function of the scaled distance from the grafting surface z/R_F. Simulation results for anchored chains ($M = 50$) of length $N = 50$ at $\rho_a\sigma^2 = 0.02$, 0.04, 0.06, 0.09, and 0.17 (from top to bottom).

surface. After a long equilibration run (typically of the order 10^6 time steps), the average monomer profile $\rho(z)$ becomes stable and measurement runs were carried out over a time of typically $1.5 \times 10^4\tau$.

IV. Results and Discussion

The theoretically predicted scaling law of the brush height $h \sim N\rho_a^{1/3}$ has been confirmed in several simulations (see, e.g., refs 13, 14, and 17). Provided ρ_a is above the critical overlap density $\rho_a^* \sim N^{-6/5}$ the brush size, as measured by the first moment of the monomer density distribution $h = \int z\rho(z)\,dz/\int\rho(z)\,dz$, approaches the predicted scaling form. Figure 4 shows this behavior in an appropriate scaling plot of the brush height and the z-component of the radius of gyration $R_{G,z} \equiv 1/(N+1)\langle\sum_{i=0}^{N}(z_i - z_{cm})^2\rangle^{1/2}$, where z_{cm} is the z-coordinate of the center of mass. The horizontal scaling variable is chosen as $N(\rho_a a^2)^{1/3}/R_F$. The scaling arguments presented in section II show that this ratio scales as $N(\rho_a a^2)^{1/3}/R_F \sim \beta^{1/2}$. Note that in the simulation model the Flory radius obeys $R_F \sim N^{3/5}$. In this way we obtain a universal crossover point $N(\rho_a^* a^2)^{1/3}/R_F \approx 1.4$. This is consistent with the estimation $N\rho_a^{1/3} \gtrsim 15$ given by Murat and Grest[17] for $N = 50$. Thus, for the chain length $N = 50$, the case we will discuss primarily in the following, the asymptotic scaling regime is reached for higher surface coverages (see Figure 4). Figure 5 shows the behavior of the reduced monomer density $\rho(z)/N\rho_a$ at increasing anchoring density. The stretching of the chains with increasing surface coverage is evident. In Figure 6 we plot the effective stretching factor $\gamma(\rho_a) = \langle z_e(\rho_a)\rangle/\langle z_{e,\text{single chain}}\rangle$, i.e., the chain stretching in the brush compared to that of a single end-grafted chain (see eq 8), versus the rescaled anchoring density $[N(\rho_a a^2)^{1/3}/R_F]^2 \sim \beta$. The scaling behavior is reasonable and quite similar to that predicted by the SCF theory (see Figure 2). Thus, for the parameter range under discussion the theoretical stretching parameter β is of the order $1 < \beta < 20$. We remember that, following Figure 4, the scaling regime is expected to occur at $N(\rho_a^* a^2)^{1/3}/R_F \gtrsim 1.4$. Thus, using Figure 6 as a calibration curve, one can conclude that this regime is likely to be reached at an effective chain stretching $\gamma \gtrsim 1.5$.

In agreement with the SCF profiles shown in Figure 1, the monomer density decays smoothly to zero at distances far from the anchoring plane. However, comparing the shape of the profiles in more detail, there appears a clear difference. Our simulation results as

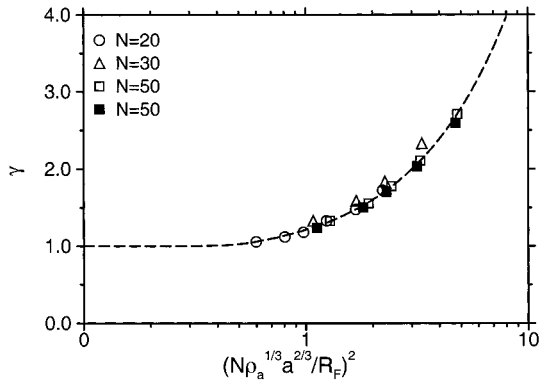

Figure 6. Effective stretching factor γ as a function of the rescaled anchoring density $[N(\rho_a a^2)^{1/3}/R_F]^2$. Simulation results with the dashed line being a guide to the eyes (full symbols $M = 50$, strong FENE; open symbols $M = 6$, weak FENE).

well as previous results by Murat and Grest[17] show the presence of a region over which the monomer profiles become rather flat for anchoring densities $\rho_a \gtrsim 0.1\sigma^{-2}$. According to Figure 6 and Figure 2, respectively, this corresponds to stretching factors $\gamma \gtrsim 2$ or $\beta \gtrsim 10$. On the other hand, the SCF profiles do not indicate such a behavior. This discrepancy between results obtained on the basis of interaction potentials that contain higher order terms in the virial expansion (like in the simulation model) and results found by means of Hamiltonians that do not contain such terms (like in the SCF model) was already pointed out before by Zuckermann and coworkers.[13] The conditional polymer paths $\langle z_{z_e}(n)\rangle/\langle z_e\rangle$ with $1 \le n \le N$ ($N = 50$), i.e., averaging over a subset of those trajectories which end at a certain distance from the grafting plane $z_e < z' < z_e + dz_e$, together with the corresponding normalized density of free ends $\rho_e(z)$ are shown in Figure 7 for three typical anchoring densities corresponding to stretching factors $\gamma \approx 1.3$, 1.8, and 2.7. The trajectories are very similar to those predicted by the SCF theory (see Figure 3). Paths which end far from the anchoring surface are stretched through their entire length, including the free end point. The paths which end farthest from the wall are almost uniformly stretched and appear almost as a straight line. On the other hand, paths which end close to the anchoring surface are nonmonotonic, first moving away from the wall, reaching a maximum, and then turning back toward the anchoring surface. Except at the maximum separation

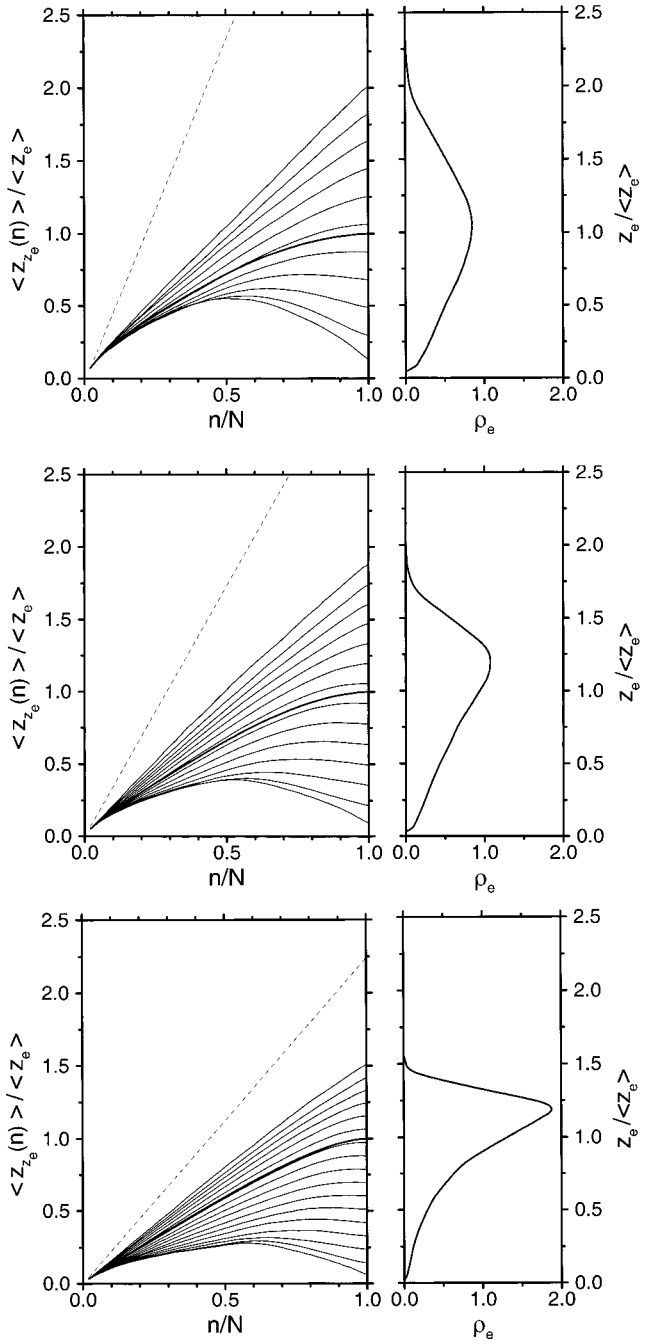

Figure 7. Conditional average height of monomers $\langle z_{z_e}(n)\rangle/\langle z_e\rangle$ for polymer paths which end at a certain distance $z_e < z' < z_e + dz_e$ from the wall as a function of n/N ($N = 50$, $M = 50$) (on the left) and the density of free ends ρ_e versus scaled end-point position $z_e/\langle z_e\rangle$ (on the right). Simulation results with anchoring densities $\rho_a\sigma^2 = 0.02$, 0.06, and 0.17 (from top to bottom) corresponding to stretching factors $\gamma \approx 1.3$, 1.8, 2.7. The thick solid lines show the mean paths obtained by averaging over all end-point positions. The thin dashed lines correspond to the hypothetical path with maximum end-point distance at fixed average bond length $a \approx 0.97\sigma$.

from the surface, these paths are stretched everywhere, including the end point. These results agree qualitatively quite well with the SCF theory. However, they seem to contradict previous numerical SCF results[10] which appear to show that the polymer paths are unstretched at the free end, in apparent agreement with ISL theory of Milner, Witten, and Cates[2] and Zhulina and co-workers.[1] However, we believe that in ref 10 the average was taken over all polymer paths, regardless

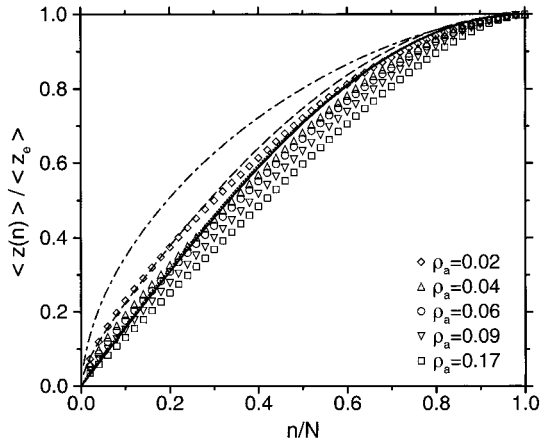

Figure 8. Scaled average height of monomers $\langle z(n)\rangle/\langle z_e\rangle$ as a function of n/N. Simulation results (symbols) for the same cases as in Figure 5, SCF results for $\beta = 1$ (dot−dashed), $\beta = 10$ (dashed), $\beta = 100$ (doted) (see Figure 3), and ISL prediction (solid curve) following from eq 20.

of their end-point position z_e. As can be seen from Figure 3 as well as from Figure 7, the stretching, proportional to (dz/dt) or (dz/dn), respectively, is positive for some particular paths and negative for others, so that the average, plotted as thick line in the figures, can be rather small. Figure 8 shows these average trajectories, i.e., the scaled mean distance of the nth monomer from the wall $\langle z(n)\rangle/\langle z_e\rangle$ obtained after averaging over all end points, together with SCF results for three different values of β (see Figure 3) and the ISL prediction

$$\langle z(n)\rangle = \langle z_e\rangle \sin\frac{n\pi}{2N} \tag{20}$$

On the one hand, the figure clearly shows that the end-point stretching of the mean polymer paths actually vanishes or becomes very small if the average is taken over all polymer paths. On the other hand, the agreement with both SCF and ISL results is rather poor. In contradiction to general arguments as well as to previous simulation results,[13] it becomes even worse with increasing coverage. As pointed out above, this discrepancy is likely to occur due to higher order interactions being present in our simulation model. Indeed, replotting the mean polymer paths obtained in a very similar model by Neelov and Binder[15] (their Figure 4), one obtains a behavior showing actually the same tendencies as Figure 8. Note that the average path for $\beta = 100$ is almost not distinguishable from the infinite-stretching limit. As noted by Johner and Joanny,[19] within the Gaussian classical approximation the end-point stretching $\pi(z_e)$ is related to the logarithmic derivative of the end-point distribution by the relation[4]

$$\pi(\tilde{z}_e) \equiv \frac{d\tilde{z}(t)}{dt}\Big|_{t=1} = -\frac{1}{2\beta}\frac{d\ln\rho_e(\tilde{z}_e)}{d\tilde{z}_e} \tag{21}$$

In agreement with the ISL theory eq 21 yields vanishing end-point stretching in the limit $\beta \to \infty$. To apply the relation directly to simulation results, it is rewriten in terms of segment number n and dimensional coordinates z to give

$$\pi(z_e) \equiv \frac{dz(n)}{dn}\Big|_{n=N} = -\frac{R_F^2}{3N}\frac{d\ln\rho_e(z_e)}{dz_e} \tag{22}$$

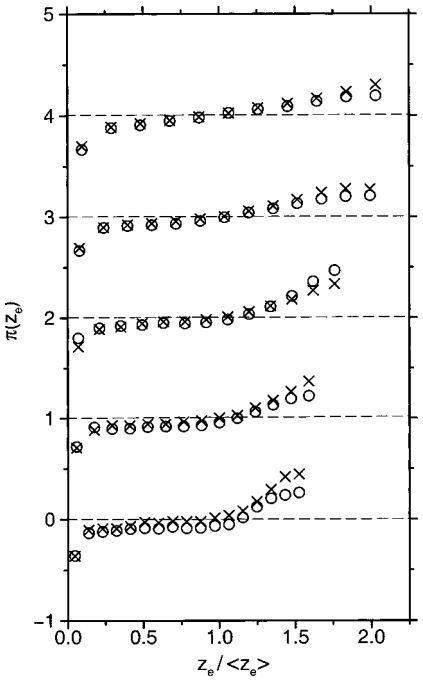

Figure 9. End-point stretching $\pi(z_e)$ as a function of the scaled distance z_e of the end points from the grafting surface taken (i) directly from the polymer paths shown in Figure 7 (×) and (ii) from the density of free ends $\rho_e(z)$ by using eq 22 (circles). Simulation results for the same cases as in Figure 5, i.e., for anchoring densities from $\rho_a\sigma^2 = 0.02$ (top) to 0.17 (bottom). Each curve is shifted vertically with respect to the previous one by 1.

The vanishing end-point stretching in the ISL limit is now hidden in the logarithmic derivative of $\rho_e(z_e)$. Figure 9 shows the end-point stretching on the one hand taken directly from the polymer paths (crosses) and on the other hand evaluated from the end-point distribution by means of eq 22 (circles) using the measured mean square end-to-end distance R_F of a free reference chain. Note that there is no fit parameter in eq 22. As long as the anchoring density is not too high, the agreement is quite good. Polymer paths ending more distant from the anchoring plane than the mean path undergo a positive end-point stretching while paths ending closer exhibit a negative one. The disagreement at higher surface coverages may be due to higher order interactions becoming important at higher monomer densities. On the other hand, Figure 9 shows that end-point stretching becomes very small with increasing anchoring density for a growing set of trajectories.

V. Conclusions

In this article we confirmed by molecular dynamics simulations that the end points of grafted polymer chains are stretched even in the presence of fluctuations, in agreement with predictions of classical[3] and self-consistent field calculations.[4] The end-point stretching is shown to change its sign with increasing separation of the free ends from the anchoring surface. Free ends point toward the wall for small separations while they point away from the wall for larger end-point distances. This finding is of clear conceptual importance, since it shows that these intricate effects exist even in the presence of density fluctuations. Furthermore, obviously the model we used for the simulations is a more realistic polymer model, including the finite extensibility of the bonds, and a monomer−monomer interaction potential incorporating the hard-core interaction. Our results show that the end-point stretching effects, which were originally predicted for a Gaussian polymer model with second-virial repulsion, are rather model independent and also occur for a more realistic polymer model. We conclude that these effects should also be present in experimental systems. To measure the end-point stretching, one would have to attach an orientationally active group to the terminal monomer of a grafted polymer chain. A convenient technique to measure the orientation of this labeled group would be, e.g., second-harmonic generation.[20] A distance-dependent measurement is then possible with an evanescent beam.

Acknowledgment. We thank F. Csajka for his support in simulating nonanchored chains and acknowledge useful discussions with W. Fenzl, H. Motschmann, and R. Teppner.

References and Notes

(1) Skvortsov, A. M.; Gorbunov, A. A.; Pavlushkov, V. A.; Zhulina, E. B.; Borisov, O. V.; Priamitsyn, V. A. *Polym. Sci. USSR* **1988**, *30*, 1706. Zhulina, E. B.; Priamitsyn, V. A.; Borisov, O. V. *Polym. Sci. USSR* **1989**, *31*, 205. Zhulina, E. B.; Borisov, O. V.; Priamitsyn, V. A. *J. Colloid Interface Sci.* **1990**, *137*, 495.

(2) Milner, S. T.; Witten, T. A.; Cates, M. E. *Europhys. Lett.* **1988**, *5*, 413. Milner, S. T.; Witten, T. A.; Cates, M. E. *Macromolecules* **1988**, *21*, 2610.

(3) Netz, R. R.; Schick, M. *Europhys. Lett.* **1997**, *38*, 37.

(4) Netz, R. R.; Schick, M. *Macromolecules* **1998**, *31*, 5105.

(5) Cosgrove, T. *J. Chem. Soc., Faraday Trans.* **1990**, *86*, 1323. Auroy, P.; Auvray, L.; Leger, L. *Phys. Rev. Lett.* **1991**, *66*, 719; *Macromolecules* **1991**, *24*, 2523; *Macromolecules* **1991**, *24*, 5158.

(6) Field, J. B.; Toprakcioglu, C.; Ball, R. C.; Stanley, H. B.; Dai, L.; Barford, W.; Penfold, J.; Smith, G.; Hamilton, W. *Macromolecules* **1992**, *25*, 434. Kent, M. S.; Lee, L.-T.; Farnoux, B.; Rondelez, F. *Macromolecules* **1992**, *25*, 6240. Factor, B. J.; Lee, L.-T.; Kent, M. S.; Rondelez, F. *Phys. Rev. E* **1993**, *48*, R2354.

(7) Hadziioannou, G.; Patel, S.; Granick, S.; Tirrell, M. *J. Am. Chem. Soc.* **1986**, *108*, 2869. Tirrell, M.; Patel, S.; Hadziioannou, G. *Proc. Natl. Acad. Sci. U.S.A.* **1987**, *84*, 4725. Watanabe, H.; Tirrell, M. *Macromolecules* **1993**, *26*, 6455.

(8) Alexander, S. *J. Phys. (Paris)* **1977**, *38*, 983.

(9) Cosgrove, T.; Heath, T.; van Lent, B.; Leermakers, F.; Scheutjens, J. *Macromolecules* **1987**, *20*, 1692. Fleer, G. J.; Cohen Stuart, M. A.; Scheutjens, J. M. H. M.; Cosgrove, T.; Vincent, B. *Polymers at Interfaces*; Chapman and Hall: London, 1993.

(10) Milner, S. T. *J. Chem. Soc., Faraday Trans.* **1990**, *86*, 1349.

(11) Orland, H.; Schick, M. *Macromolecules* **1996**, *29*, 713.

(12) Grest, G. S.; Murat, M. In *Monte Carlo and Molecular Dynamics Simulations in Polymer Science*; Binder, K., Ed.; Oxford University Press: New York, Oxford, 1995.

(13) Laradji, M.; Guo, H.; Zuckerman, M. J. *Phys. Rev. E* **1994**, *49*, 3199.

(14) Lai, P.-Y.; Binder, K. *J. Chem. Phys.* **1991**, *95*, 9288.

(15) Neelov, I. M.; Binder, K. *Macromol. Theory Simul.* **1995**, *5*, 119.

(16) Grest, G. S.; Kremer, K. *Phys. Rev. A* **1986**, *33*, 3628.

(17) Murat, M.; Grest, G. S. *Macromolecules* **1989**, *22*, 4054.

(18) Dünweg, B.; Kremer, K. *Phys. Rev. Lett* **1991**, *66*, 2996.

(19) Johner, A.; Joanny, J. F. *J. Chem. Phys.* **1993**, *98*, 1647.

(20) Harke, H.; Ibn-Elhaj, M.; Möhwald, H.; Motschmann, H. *Phys. Rev. E* **1998**, *57*, 1806.

MA981582W